

# Geometry-Based Stochastic Probability Models for the LoS and NLoS Paths of A2G Channels Under Urban Scenarios

Minghui Pang<sup>1</sup>, Qiuming Zhu<sup>1</sup>, *Member, IEEE*, Cheng-Xiang Wang<sup>1</sup>, Zhipeng Lin, *Member, IEEE*, Junyu Liu<sup>1</sup>, *Member, IEEE*, Chongyu Lv<sup>1</sup>, and Zhuo Li<sup>1</sup>, *Member, IEEE*

**Abstract**—Path probability prediction is essential to describe the dynamic birth and death of propagation paths, and build the accurate channel model for air-to-ground (A2G) communications. The occurrence probability of each path is complex and time variant due to fast changeable altitudes of unmanned aerial vehicles and scattering environments. Considering the A2G channels under urban scenarios, this article presents three novel stochastic probability models for the Line-of-Sight (LoS) path, ground specular (GS) path, and building scattering (BS) path, respectively. By analyzing the geometric stochastic information of 3-D scattering environments, the proposed models are derived with respect to the width, height, and distribution of buildings. The effect of the Fresnel zone and altitudes of transceivers are also taken into account. Simulation results show that the proposed LoS path probability model has good performance at different frequencies and altitudes and is also consistent with existing models at the low or high altitude. Moreover, the proposed LoS and

non-LoS path probability models show good agreement with the ray-tracing (RT) simulation method.

**Index Terms**—Air-to-ground (A2G) channels, channel model, Fresnel zone, ray tracing (RT), stochastic path probability.

## I. INTRODUCTION

UNMANNED aerial vehicles (UAVs) have been widely used in aerial photography, disaster rescue, and other fields due to small size, low cost, and easy deployment [1], [2], [3], [4], [5], [6]. The space-air-ground-sea integrated network is a key part of the global Internet of Things (IoT) construction, which greatly relies on the reliable air-to-ground (A2G) communication link [7], [8], [9], [10], [11], [12]. The random and dynamic birth and death of propagation paths is a big challenge to maintain the reliable A2G link [13], [14], [15], [16], [17], [18], [19], [20], [21]. Thus, accurate and general propagation path probability models are urgently needed, in order to describe the dynamic birth and death of propagation paths and improve the communication performance.

There are limited literature on the path probability prediction. Some researchers used accurate digital maps to determine the Line-of-Sight (LoS) path by geometric operation, namely, the deterministic method. This method is only suitable for a specific scenario and requires accurate maps. On the other hand, stochastic methods [22], [23], [24], [25], [26], [27], [28], [29], [30], [31], [32], [33], [34], [35], [36], [37], [38], [39], [40], [42] are more popular, which can be mainly classified into measurement-based empirical method [22], [23], [24], [25], simulation-based empirical method [26], [27], [28], [29], [30], [31], [32], [33], and geometry-based analytical method [34], [35], [36], [37], [38], [39], [40], [42].

The measurement-based empirical method and simulation-based empirical method establish the stochastic path probability models by analyzing massive measured and simulated data. There are several standard LoS probability models based on the massive measurement data under several typical scenarios in International Telecommunication Union-Radio (ITU-R) M.2135-1 [22], the Third Generation Partnership Project (3GPP) TR 38.901 [23], 5G Channel Model (5GCM) [24], and WINNER II [25]. Since it is complex and high cost to acquire measurement data, several empirical models are proposed based on simulation data, e.g., data obtained with

Manuscript received 26 August 2022; accepted 21 September 2022. Date of publication 4 October 2022; date of current version 24 January 2023. This work was supported in part by the National Key Scientific Instrument and Equipment Development Project under Grant 61827801; in part by the National Natural Science Foundation of China under Grant 62271250; in part by the Natural Science Foundation of Jiangsu Province under Grant BK20211182; in part by the Open Research Fund of National Mobile Communications Research Laboratory, Southeast University under Grant 2022D04; and in part by the Key Technologies Research and Development Program of Jiangsu (Prospective and Key Technologies for Industry) under Grant BE2022067 and Grant BE2022067-3. (Corresponding authors: Qiuming Zhu; Cheng-Xiang Wang.)

Minghui Pang and Qiuming Zhu are with the Key Laboratory of Dynamic Cognitive System of Electromagnetic Spectrum Space, College of Electronic and Information Engineering, Nanjing University of Aeronautics and Astronautics, Nanjing 211106, China, and also with the State Key Laboratory of Integrated Services Networks, Xidian University, Xi'an 710000, China (e-mail: pangminghui@nuaa.edu.cn; zhuqiuming@nuaa.edu.cn).

Cheng-Xiang Wang is with the National Mobile Communications Research Laboratory, School of Information Science and Engineering, Southeast University, Nanjing 210096, China, and also with the Pervasive Communication Research Center, Purple Mountain Laboratories, Nanjing 211111, China (e-mail: chxwang@seu.edu.cn).

Zhipeng Lin and Chongyu Lv are with the Key Laboratory of Dynamic Cognitive System of Electromagnetic Spectrum Space, College of Electronic and Information Engineering, Nanjing University of Aeronautics and Astronautics, Nanjing 211106, China (e-mail: linlzp@nuaa.edu.cn; lvcy2166@163.com).

Junyu Liu is with the State Key Laboratory of Integrated Services Networks, Xidian University, Xi'an 710000, China (e-mail: junyuliu@xidian.edu.cn).

Zhuo Li is with the Key Laboratory of Radar Imaging and Microwave Photonics, Nanjing University of Aeronautics and Astronautics, Nanjing 211106, China (e-mail: lizhuo@nuaa.edu.cn).

Digital Object Identifier 10.1109/JIOT.2022.3211524

TABLE I  
RELATED WORKS ON MEASUREMENT/SIMULATION-BASED EMPIRICAL MODEL

Methods	Models	Channels	Altitude-dependent	Frequency-dependent	LoS Probability	NLoS Probability
Measured/simulated-based empirical model	ITU-R2135 [22]	B2G	×	×	✓	×
	3GPP TR 38.901 [23]	B2G	×	×	✓	×
	5GCM [24]	B2G	×	×	✓	×
	WINNER [25]	B2G	×	×	✓	×
	Model in [28]	B2G	×	×	✓	×
	Model in [29]	B2G	×	×	✓	×
	Model in [27]	H2G	angle-dependent	×	✓	×
	Model in [31]	A2G	angle-dependent	×	✓	×
	Model in [32]	B2G	✓	×	✓	×
Model in [30]	A2G	✓	×	✓	×	

Note: B2G (base station to ground), H2G (high altitude platform to ground).

TABLE II  
RELATED WORKS ON GEOMETRY-BASED ANALYTICAL MODEL

Methods	Models	Channels	Altitude-dependent	Frequency-dependent	LoS Probability	NLoS Probability
Geometry-based analytical model	ITU-R1410 [34]	B2G	×	×	✓	×
	Model in [35]	H2G	angle-dependent	×	✓	×
	Model in [42]	A2G	angle-dependent	×	✓	×
	Model in [41]	A2G	✓	×	✓	×
	Model in [39]	A2G	✓	×	✓	×
	Model in [36]	A2G	✓	×	✓	×
	Model in [40]	A2G	✓	✓	✓	×
	Model in [37]	B2G	✓	✓	✓	×
	Model in [38]	B2G	✓	✓	✓	×
The proposed model	A2G	✓	✓	✓	✓	

ray-tracing (RT) method [26], [27], [28], [29], [30], [31], [32], and data obtained with point cloud method [33]. Table I summarizes the related works on the measurement-based and simulation-based empirical model. The accuracy of this kind of model greatly depends on the original data and it usually requires a large amount of computations.

The geometry-based analytical method predicts the path probability by applying the electromagnetic wave propagation theory and geometry information. Especially, the scenarios are described in a stochastic way according to the stochastic properties of buildings [34], [35], [36], [37], [38], [39], [40], [42]. Specifically, a well-known analytical method was proposed in ITU-R Rec. P.1410 [34], which utilized three stochastic geometry parameters to define different urban scenarios. The buildings were distributed uniformly and the height of buildings followed Rayleigh distribution. On this basis, several LoS probability models were addressed in [35], [36], [37], [38], [39], and [40]. For example, Al-Hourani et al. [35] proposed an LoS probability model with respect to the elevation angle. However, the model was only appropriate for the altitude of troposphere (over 10 km). Recently, an elevation angle-related LoS probability model for the UAV-to-ground (U2G) urban

scenarios was proposed in [36]. Furthermore, considering the factor of the Fresnel zone, Liu et al. [37] and Cui et al. [38] proposed frequency-dependent LoS probability models. Gapeyenko et al. [39] proposed an altitude-dependent LoS probability model for UAV communications. Zhu et al. [40] proposed an altitude-dependent and frequency-dependent LoS probability models for A2G communications and obtained the closed expression. In addition, the prediction model in [41] described the buildings by cylinders following Poisson distribution, and the height obeyed the Log-normal distribution. Another altitude-dependent LoS probability model based on the Poisson distribution of buildings can be addressed in [42]. Table II summarizes the representative works on the geometry-based analytical model. As we can see, few models can be applied to the wide range of altitude. In addition, the frequency factor is usually not considered. Moreover, to the best knowledge of the authors, the aforementioned models only consider the LoS probability, while the non-LoS (NLoS) path, including the ground specular (GS) path and building scattering (BS) path, is rarely involved. This article aims to fill this gap and build the stochastic altitude-dependent and frequency-dependent probability models for different paths.

The main novelties and contributions are summarized as follows.

- 1) A general stochastic prediction model for the LoS probability of A2G channels in urban scenarios is proposed. This model takes the factors of transceiver altitude, building height, building width, building location, and the Fresnel zone into account, which makes it general and suitable for different altitudes and frequencies.
- 2) Geometry-based stochastic probability models for the GS and BS paths in urban scenarios are proposed for the first time. We adopt the research methods of mirror scenario analysis and the first Fresnel zone restriction and consider the effect of Fresnel ellipsoids and the geometric stochastic information, such as transceiver locations and distribution of buildings. The two proposed models can be adapted to different heights, frequencies, and urban scenarios.
- 3) Based on the stochastic scenario-dependent parameters, we construct virtual urban scenarios and obtain the LoS, GS, and BS path probabilities by averaging massive RT simulation. The simulation results show that the proposed models have good agreement with the RT data. The proposed model is also consistent with existing models at low or high altitude. In addition, we analyze the influence factors and average maximum communication distance (MCD) based on the proposed path probability models.

The remainder of this article is organized as follows. Section II demonstrates the propagation process and analyzes the factors that affect the occurrence probability. In Section III, the probability models of LoS, GS, and BS paths are analyzed and derived for typical urban scenarios. The comparisons and validations are given in Section IV. Finally, conclusions are drawn in Section V.

## II. PROPAGATION PATH OF A2G CHANNELS

The A2G channel generally consists of an LoS path and several NLoS paths, i.e., the GS paths and BS paths. Mao et al. [19] mentioned that the sum power of LoS path, GS path, and BS path with the largest power exceeds 99% of the total received power. Therefore, the channel impulse response (CIR) can be simplified as

$$\sigma(\tau, t) = \sigma^{\text{LoS}}(t) + \sigma^{\text{GS}}(\tau, t) + \sigma^{\text{BS}}(\tau, t) \quad (1)$$

where  $\sigma^{\text{LoS}}(t)$ ,  $\sigma^{\text{GS}}(\tau, t)$ , and  $\sigma^{\text{BS}}(\tau, t)$  denote the CIRs of LoS, GS, and BS paths. Note that the occurrence of each path is random, which mainly depends on the scattering environment and locations of transceivers. This article focuses on predicting the occurrence of each path in a stochastic way, denoted by the path probabilities as  $p^{\text{LoS}}$ ,  $p^{\text{GS}}$ , and  $p^{\text{BS}}$ , respectively.

In order to build the probability model, we first need to describe the scattering scenario in a stochastic way. In this article, we adopt the well-known classification and description method in [27] and [34]. The method divides the urban scenarios into four typical categories, i.e., Suburban, Urban, Dense urban, and High-rise urban. Four typical categories are

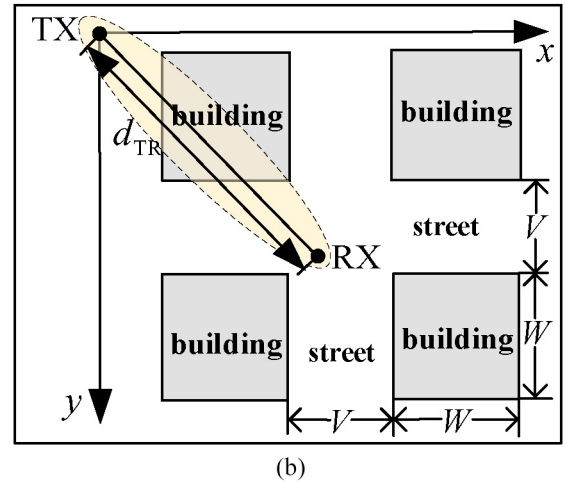
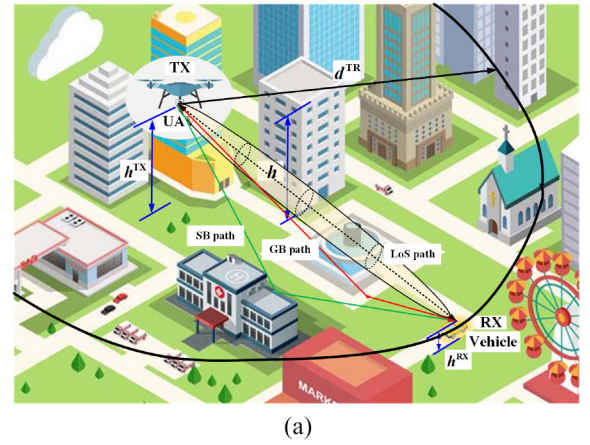


Fig. 1. Illustration of propagation paths of an A2G urban channel. (a) 3-D view of a typical A2G channel. (b) 2-D view of a typical A2G channel.

described by three parameters  $\{\alpha, \beta, \gamma\} \in \psi$ , where  $\alpha$  is the percentage of land area covered by buildings,  $\beta$  represents the density of buildings, and  $\gamma$  denotes the mean value of random building height. The three parameters of the Suburban, Urban, Dense urban, and High-rise urban are (0.1, 750, 8), (0.3, 500, 15), (0.5, 300, 20), and (0.5, 300, 50). The location of buildings follows Uniform distribution and the mean value of building width in these four scenarios are 11.6, 24.5, 40.8, and 40.8 m, respectively. The height of buildings follows Rayleigh distribution as

$$F(h) = \frac{h}{\gamma^2} \exp\left[-\frac{(h)^2}{2\gamma^2}\right] \quad (2)$$

where  $h$  is the height of buildings.

A typical A2G channel under urban scenarios is shown in Fig. 1, where  $h^{\text{TX}}$  and  $h^{\text{RX}}$  represent the heights of transmitter (TX) and receiver (RX), respectively, and  $d^{\text{TR}}$  is the horizontal distance between TX and RX. In the figure, the average building width [43] can be obtained by

$$W = 1000\sqrt{\alpha/\beta} \quad (3)$$

and the average street width can be obtained by

$$V = 1000/\sqrt{\beta} - W. \quad (4)$$

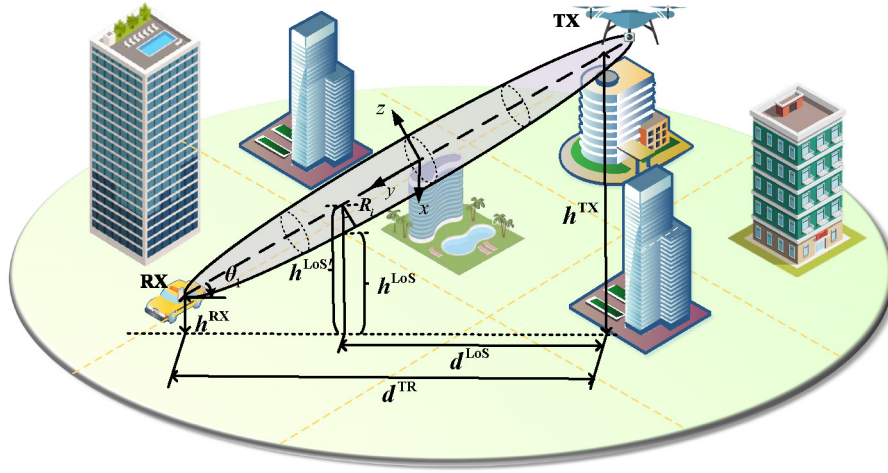


Fig. 2. LoS path of A2G channel under urban scenarios.

The average number of buildings along the propagation path between the transceivers can be calculated by

$$E[N] = \text{floor}(d^{\text{TR}} \sqrt{\alpha\beta}/1000) \quad (5)$$

where  $\text{floor}(\cdot)$  represents the downward rounding function.

The energy of the propagation path is not concentrated along a straight line but in the entire Fresnel zone. When we consider the occurrence of the propagation path, it is necessary to judge the occlusion of obstacles not only along the straight path but also on the entire Fresnel zone. The Fresnel clearance zone can be expressed as [37], [38]

$$\frac{x^2}{X^2} + \frac{y^2}{Y^2} + \frac{z^2}{Z^2} \leq 1 \quad (6)$$

where the ellipsoid parameters can be calculated by

$$\begin{cases} X = Z = \frac{\sqrt{\lambda d^{\text{TR}}}}{2} \\ Y = \sqrt{\frac{\lambda d^{\text{TR}}}{4} + \frac{(d^{\text{TR}})^2}{4}} \end{cases} \quad (7)$$

where  $\lambda$  is the wavelength. In this article, we only consider the first-order Fresnel zone which includes half of total field strength. The radius of the first-order Fresnel ellipsoid corresponding to the location of the  $i$ th building is

$$R_i = \begin{cases} \frac{\sqrt{\lambda d^{\text{TR}} d_i}}{d^{\text{TR}}}, & d_i \leq \frac{d^{\text{TR}}}{2} \\ \frac{\sqrt{\lambda d^{\text{TR}} (d^{\text{TR}} - d_i)}}{d^{\text{TR}}}, & d_i > \frac{d^{\text{TR}}}{2} \end{cases} \quad (8)$$

where  $d_i$  is the distance between the  $i$ th building and TX, given by

$$d_i = \frac{(i - 0.5)d^{\text{TR}}}{\text{floor}(d^{\text{TR}} \sqrt{\alpha\beta}/1000)} + \frac{W}{2}. \quad (9)$$

### III. STOCHASTIC PATH PROBABILITY MODELS

#### A. LoS Path Probability Model

Most of the scatterers under A2G communication scenarios are on the ground and the LoS propagation is cut off only when the Fresnel zone is totally blocked by obstacle as shown in Fig. 2. In other words, the Fresnel zone between TX and

RX is not blocked by any building. Thus, the LoS probability can be defined as

$$P^{\text{LoS}} = \prod_{i=1}^{E[N]} P_i^{\text{LoS}} = \prod_{i=1}^{E[N]} P(h_i < h_i^{\text{LoS}}) \quad (10)$$

where  $P_i^{\text{LoS}}$  is the probability that the  $i$ th building does not block the LoS path,  $h_i$  is the height of the  $i$ th building, and  $h_i^{\text{LoS}}$  is the maximum height of the  $i$ th building unblocking the LoS path.

Since the height of buildings follows the Rayleigh distribution, the probability that the buildings do not block the LoS path is

$$P_i^{\text{LoS}} = P(h_i < h_i^{\text{LoS}}) = \int_0^{h_i^{\text{LoS}}} F(h) dh = 1 - \exp\left[-\frac{(h_i^{\text{LoS}})^2}{2\gamma^2}\right]. \quad (11)$$

When the effect of the Fresnel ellipsoid is not considered, the maximum height point is along the straight line between TX and RX, which can be expressed as

$$h_i^{\text{LoS}'} = h^{\text{TX}} - \frac{d_i(h^{\text{TX}} - h^{\text{RX}})}{d^{\text{TR}}}. \quad (12)$$

The influence of Fresnel ellipsoid depending on the signal frequency is considered in this article. The maximum height can be modified as the lowest point of the first-order Fresnel zone as shown in Fig. 2. It yields

$$h_i^{\text{LoS}} = h^{\text{TX}} - \frac{d_i(h^{\text{TX}} - h^{\text{RX}})}{d^{\text{TR}}} - \frac{R_i}{\cos \theta_1}. \quad (13)$$

Furthermore, we can obtain

$$\cos \theta_1 = \frac{d^{\text{TR}}}{\sqrt{(d^{\text{TR}})^2 + (h^{\text{TX}} - h^{\text{RX}})^2}}. \quad (14)$$

Finally, the LoS probability can be obtained by (15), shown at the bottom of the next page, which is related to the altitudes of TX and RX, the communication frequency, and the scenario.

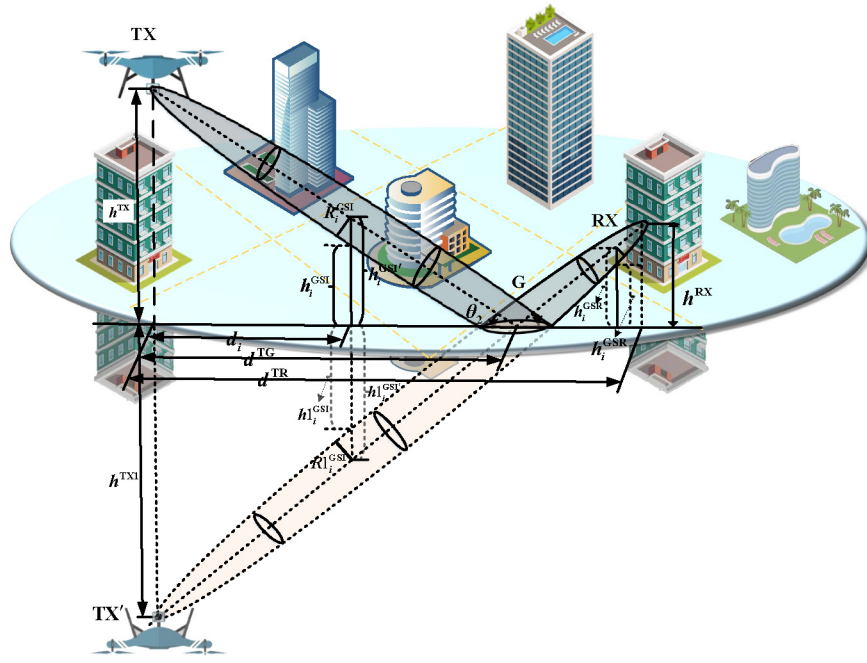


Fig. 3. GS path of A2G channel under urban scenarios.

### B. GS Path Probability Model

The GS propagation path consists of three parts, i.e., the incident path, reflection path, and Fresnel reflection zone. The location and height of buildings obey the aforementioned distributions. As shown in Fig. 3, the area under the ground is the mirror of the counterpart above the ground. The area that the Fresnel ellipsoid between mirrored TX' and RX crosses the ground can be denoted by  $G$ , i.e., the reflection Fresnel zone. Then, the probability that the  $i$ th building does not block the GS path can be equivalent to the LoS probability between RX and mirrored TX' as shown in Fig. 3. Thus, it can be expressed as

$$P_i^{\text{GS}} = P(h_i < h_i^{\text{GS}}) = \int_0^{h_i^{\text{GS}}} F(h) dh = 1 - \exp\left[-\frac{(h_i^{\text{GS}})^2}{2\gamma^2}\right]. \quad (16)$$

However, it is slightly different from calculating LoS probability, since the buildings are divided into two classes according to their positions in this article. Therefore, the GS path exists only when the building between TX and  $G$  does not block the incident path, and the building between  $G$  and RX does not block the reflection path. Note that the case of reflection zone  $G$  not blocked by any building is already included in the above two constraints. The distance between  $G$  and TX

can be obtained by performing the triangle similarity theorem as

$$d^{\text{TG}} = \frac{d^{\text{TR}} h^{\text{TX}}}{h^{\text{TX}} + h^{\text{RX}}}. \quad (17)$$

Then, the cosine of  $\theta_2$  in Fig. 3 can be obtained as

$$\cos \theta_2 = \frac{d^{\text{TR}}}{\sqrt{(d^{\text{TR}})^2 + (h^{\text{TX}} + h^{\text{RX}})^2}}. \quad (18)$$

First, we assume that the arbitrary building is located between the TX and  $G$ , and then, the average number of buildings along the incident path can be calculated by

$$E[N^{\text{I}}] = \text{floor}(d^{\text{TG}} \sqrt{\alpha\beta}/1000). \quad (19)$$

The distance  $d_i$  between TX and the  $i$ th building can be expressed as

$$d_i < d^{\text{TG}} = \frac{d^{\text{TR}} h^{\text{TX}}}{h^{\text{RX}} + h^{\text{TX}}}. \quad (20)$$

The height of the centerline of incident Fresnel ellipsoid  $h_i^{\text{GS}'}$  is the same as the height when the incident path is considered as a straight line. It can be given by

$$h_i^{\text{GS}'} = \frac{h^{\text{TX}}(d^{\text{TG}} - d_i)}{d^{\text{TG}}}. \quad (21)$$

$$P^{\text{LoS}}(d^{\text{TR}}, h^{\text{TX}}, h^{\text{RX}}, \psi, \lambda) = \prod_{i=1}^{E[M]} \left[ 1 - \exp\left(-\frac{\left[h^{\text{TX}} - \frac{d_i(h^{\text{TX}} - h^{\text{RX}})}{d^{\text{TR}}} - \frac{\sqrt{\lambda} d^{\text{TR}} \sqrt{(d^{\text{TR}})^2 + (h^{\text{TX}} - h^{\text{RX}})^2}}{(d^{\text{TR}})^2} \min(d_i, d^{\text{TR}} - d_i)\right]^2}{2\gamma^2}\right) \right] \quad (15)$$

Considering the influence of the Fresnel zone, the maximum height at which the  $i$ th building does not block the incident path is

$$h_i^{\text{GSI}} = h_i^{\text{GSI}'} - \frac{R_i}{\cos \theta_2}. \quad (22)$$

The probability of the  $i$ th building does not block the incident ray can be derived as (23), shown at the bottom of the page.

Second, if the building is located between the RX and G, the average number of buildings along the reflection path can be calculated by

$$E[N^{\text{R}}] = \text{floor}\left(\left(d^{\text{TR}} - d^{\text{TG}}\right)\sqrt{\alpha\beta}/1000\right). \quad (24)$$

The distance  $d_i$  between the TX and the  $i$ th building can be expressed as

$$d_i > d^{\text{TG}} = \frac{d^{\text{TR}}h^{\text{TX}}}{h^{\text{RX}} + h^{\text{TX}}}. \quad (25)$$

Similarly, we can obtain

$$h_i^{\text{GSR}'} = \frac{h^{\text{RX}}(d_i - d^{\text{TG}})}{d^{\text{TR}} - d^{\text{TG}}} \quad (26)$$

and

$$h_i^{\text{GSR}} = h_i^{\text{GSR}'} - \frac{R_i}{\cos \theta_2}. \quad (27)$$

Then, the probability that the  $i$ th building does not block the reflection path can be obtained as (28), shown at the bottom of the page. Thus, the final probability model of the GS path can be obtained as

$$P^{\text{GS}}(d^{\text{TR}}, h^{\text{TX}}, h^{\text{RX}}, \psi, \lambda) = \prod_{i=1}^{E[N^{\text{I}}]} P_i^{\text{GSI}} \prod_{i=1}^{E[N^{\text{R}}]} P_i^{\text{GSR}}. \quad (29)$$

It should be noted that the case of buildings on the reflection Fresnel zone is included in (29). Since buildings are usually much larger than the reflection Fresnel zone, they would block the incident path or reflection path when close to the reflection zone.

### C. BS Path Probability Model

Since the double-bounce and multiple-bounce scattering paths have much lower power compared with the single-bounce scattering path, they are not considered in this article. Moreover, any one building can become a scattering zone when the height of the building enters the first Fresnel zone. A typical BS path in A2G communications is shown in Fig. 4. According to the position of the scattering zone, the buildings along the straight line can be classified into three categories, e.g., scattering buildings, front buildings, and behind buildings. Note that the scattering occurs on the scattering buildings. The front buildings are located between TX and the scattering zone, and the behind buildings are located between RX and the scattering zone.

During the scattering propagation process, it is necessary to ensure that the incident and scattering buildings do not block the incident path and the scattering path. Therefore, the BS probability model can be expressed as

$$P^{\text{BS}} = 1 - \prod_{i=1}^{E[N]} \left[ 1 - P_i^{\text{S}} \cdot \left( \prod_{m=1}^{E[N^{\text{F}}]} P_{i,m}^{\text{F}} \right) \cdot \left( \prod_{n=1}^{E[N^{\text{B}}]} P_{i,n}^{\text{B}} \right) \right] \quad (30)$$

where  $E[N^{\text{F}}]$  is the average number of front buildings. When the scattering zone is on the  $i$ th building, it can be expressed as

$$E[N^{\text{F}}] = \text{floor}\left(d_i\sqrt{\alpha\beta}/1000\right). \quad (31)$$

The average number of behind buildings can be obtained as

$$E[N^{\text{B}}] = \text{floor}\left[\left(d^{\text{TR}} - d_i\right)\sqrt{\alpha\beta}/1000\right]. \quad (32)$$

Then, the probability that the  $i$ th building enters the Fresnel zone can be derived as

$$P_i^{\text{S}} = P\left(h_i > h_i^{\text{S}}\right) = 1 - \int_0^{h_i^{\text{S}}} F(h)dh = \exp\left[-\frac{(h_i^{\text{S}})^2}{2\gamma^2}\right]. \quad (33)$$

According to (13) and (14), the minimum height of the  $n$ th building entering the first Fresnel ellipsoid is

$$h_i^{\text{S}} = h^{\text{TX}} - \frac{d_i(h^{\text{TX}} - h^{\text{RX}})}{h^{\text{RX}}} - \frac{R_i}{\cos \theta_3}. \quad (34)$$

$$P_i^{\text{GSI}}(d^{\text{TR}}, h^{\text{TX}}, h^{\text{RX}}, \psi, \lambda) = 1 - \exp\left(-\frac{\left[\frac{h^{\text{TX}}(d^{\text{TG}} - d_i)}{d^{\text{TG}}} - \frac{\sqrt{n\lambda d^{\text{TR}}}\sqrt{(d^{\text{TR}})^2 + (h^{\text{TX}} + h^{\text{RX}})^2}}{(d^{\text{TR}})^2} \min(d_i, d^{\text{TR}} - d_i)\right]^2}{2\gamma^2}\right) \quad (23)$$

$$P_i^{\text{GSR}}(d^{\text{TR}}, h^{\text{TX}}, h^{\text{RX}}, \psi, \lambda) = 1 - \exp\left(-\frac{\left[\frac{h^{\text{RX}}(d_i - d^{\text{TG}})}{d^{\text{TR}} - d^{\text{TG}}} - \frac{\sqrt{n\lambda d^{\text{TR}}}\sqrt{(d^{\text{TR}})^2 + (h^{\text{TX}} + h^{\text{RX}})^2}}{(d^{\text{TR}})^2} \min(d_i, d^{\text{TR}} - d_i)\right]^2}{2\gamma^2}\right) \quad (28)$$

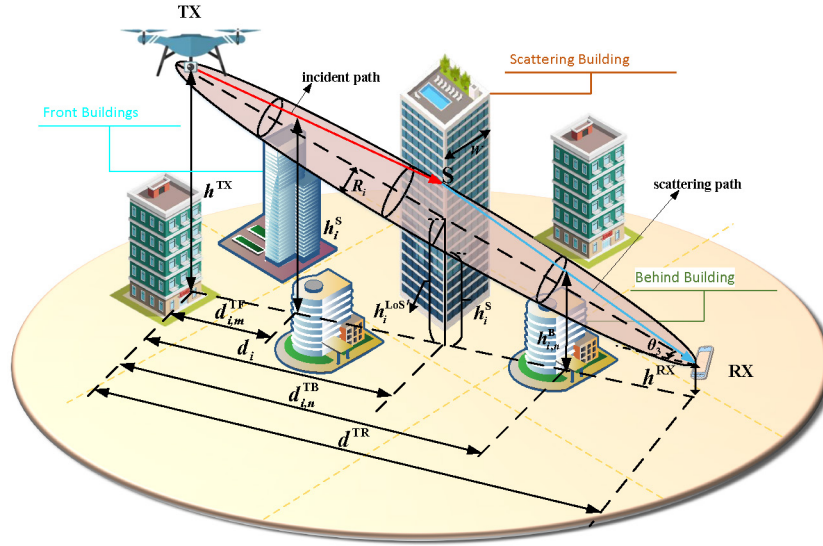


Fig. 4. BS path of A2G channel under urban scenarios.

According to triangular geometry, the cosine of  $\theta_3$  in Fig. 4 can be expressed as

$$\cos \theta_3 = \frac{d^{\text{TR}}}{\sqrt{(d^{\text{TR}})^2 + (h^{\text{TX}} - h^{\text{RX}})^2}}. \quad (35)$$

Therefore, the probability that the  $i$ th building height enters the Fresnel ellipsoid can be calculated as (36), shown at the bottom of the page.

The probability that the  $m$ th front building does not block the incident path can be expressed as

$$P_{i,m}^F = P(h_{i,m} < h_{i,m}^F) = \int_0^{h_{i,m}^F} F(h) dh = 1 - \exp\left[-\frac{(h_{i,m}^F)^2}{2\gamma^2}\right]. \quad (37)$$

Here, the maximum height of the  $m$ th front building  $h_{i,m}^F$  can be expressed as

$$h_{i,m}^F = \frac{(d_i - d_{i,m}^{\text{TF}})(h^{\text{TX}} - h_i^S)}{d_i} + h_i^S \quad (38)$$

where  $d_{i,m}^{\text{TF}}$  is the horizon distance between TX and the  $m$ th front building

$$d_{i,m}^{\text{TF}} = \frac{(i - 0.5)d_i}{\text{floor}(d_i\sqrt{\alpha\beta}/1000)} + \frac{W}{2}. \quad (39)$$

Then, the probability that the  $m$ th front building does not block the incident ray can be obtained as

$$P_{i,m}^F(d^{\text{TR}}, h^{\text{TX}}, h^{\text{RX}}, \psi, \lambda) = 1 - \exp\left(-\frac{\left[\frac{(d_i - d_{i,m}^{\text{TF}})(h^{\text{TX}} - h_i^S)}{d_i} + h_i^S\right]^2}{2\gamma^2}\right). \quad (40)$$

The probability that the  $n$ th behind the building does not block the scattering path can be defined as

$$P_{i,n}^B = P(h_{i,n} < h_{i,n}^B) = \int_0^{h_{i,n}^B} F(h) dh = 1 - \exp\left[-\frac{(h_{i,n}^B)^2}{2\gamma^2}\right] \quad (41)$$

where  $h_{i,n}^B$  denotes the maximum height of the  $n$ th front building. Similarly, we can obtain

$$P_{i,n}^B(d^{\text{TR}}, h^{\text{TX}}, h^{\text{RX}}, \psi, \lambda) = 1 - \exp\left(-\frac{\left[h^{\text{RX}} + \frac{(d^{\text{TR}} - d_{i,n}^{\text{TB}})(h^{\text{TX}} - h_i^S)}{d^{\text{TR}} - d_i}\right]^2}{2\gamma^2}\right) \quad (42)$$

where the horizon distance between TX and the  $n$ th front building can be expressed as

$$d_{i,n}^{\text{TB}} = \frac{(i - 0.5)d_i}{\text{floor}(d_i\sqrt{\alpha\beta}/1000)} + \frac{W}{2}. \quad (43)$$

$$P_i^S(d^{\text{TR}}, h^{\text{TX}}, h^{\text{RX}}, \psi, \lambda) = \exp\left(-\frac{\left[h^{\text{TX}} - \frac{d_i(h^{\text{TX}} - h^{\text{RX}})}{d^{\text{TR}}} - \frac{\sqrt{\lambda d^{\text{TR}}}\sqrt{(d^{\text{TR}})^2 + (h^{\text{TX}} - h^{\text{RX}})^2}}{(d^{\text{TR}})^2} \min(d_i, d^{\text{TR}} - d_i)\right]^2}{2\gamma^2}\right) \quad (36)$$

TABLE III  
RT SIMULATION PARAMETERS

Parameter	Value
Scenario	Suburban, Urban, Dense urban and High-rise urban
Building area ratio ( $\alpha$ )	0.1, 0.3, 0.5, 0.5
Number of buildings ( $\beta$ )	750/km <sup>2</sup> , 500/km <sup>2</sup> , 300/km <sup>2</sup> , 300/km <sup>2</sup>
Average building height ( $\gamma$ )	8 m, 15 m, 20 m, 50 m
Building width ( $W$ )	11.6 m, 24.5 m, 40.8 m, 40.8 m
Street width ( $V$ )	24.9 m, 20.2 m, 16.9 m, 16.9 m
Building location distribution	Uniform distribution
Building height distribution	Rayleigh distribution
Frequency ( $f$ )	28 GHz, 1.4 GHz, 5 GHz
Antenna type	Omnidirectional
TX altitude (interval)	0–1000 m (20 m)
TX number	1000 (50 altitudes, 20 per altitude)
RX altitude	2 m
RX number	6825 (39 concentric circles, 30-200 on each circle)

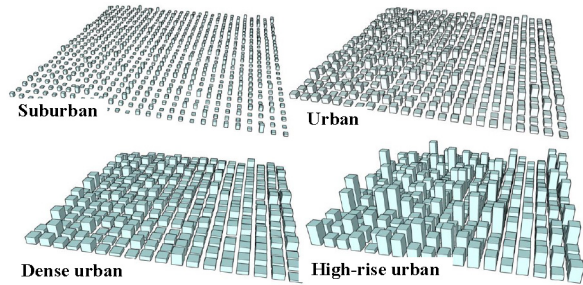


Fig. 5. Four constructed urban scenarios.

By substituting (31)–(33), (40), and (43) into (30), we can obtain the BS probability model of a single bounce.

Most of the urban scenarios can be approximately represented by one of four typical scenarios, so the scenario parameters in Section II and Table III can be used directly for prediction. For the high-precision application, users can calculate  $\psi \in \{\alpha, \beta, \gamma, W, \text{ and } V\}$  via the digital map of given scenario and substitute them into the prediction model.

#### IV. SIMULATION RESULTS AND VALIDATION

##### A. RT-Based Simulation Method

This section demonstrates the effectiveness and accuracy of proposed stochastic probability models. We conduct massive RT simulations under urban scenarios for quantitative comparison. In order to obtain the average probabilities by the RT simulation method, we first reconstruct four typical urban scenarios. These scenarios can be quantitatively described by three parameters  $\psi \in \{\alpha, \beta, \gamma\}$  and the corresponding values can be addressed in [27], [34], [35], and [38]. The reconstructed scenarios, including standard Suburban, Urban, Dense

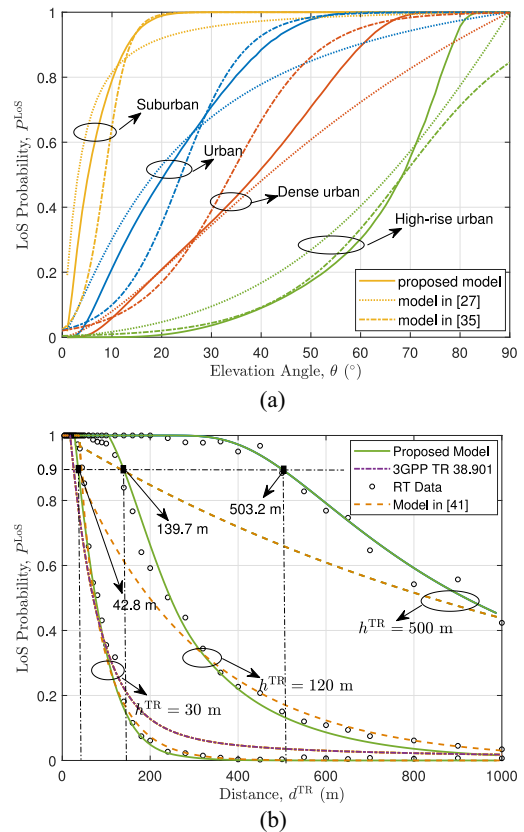


Fig. 6. Comparison of the proposed LoS probability model and RT data. (a) LoS probability versus elevation angle ( $f = 28$  GHz,  $h^{TR} = 5000$  m). (b) LoS probability versus distance ( $f = 28$  GHz,  $h^{TR} = 30, 120, 500$  m, urban scenario).

urban, and High-rise urban, are shown in Fig. 5. In the simulation, we further introduce two parameters, i.e., the building width  $W$  and the street width  $V$ . Note that their values can be

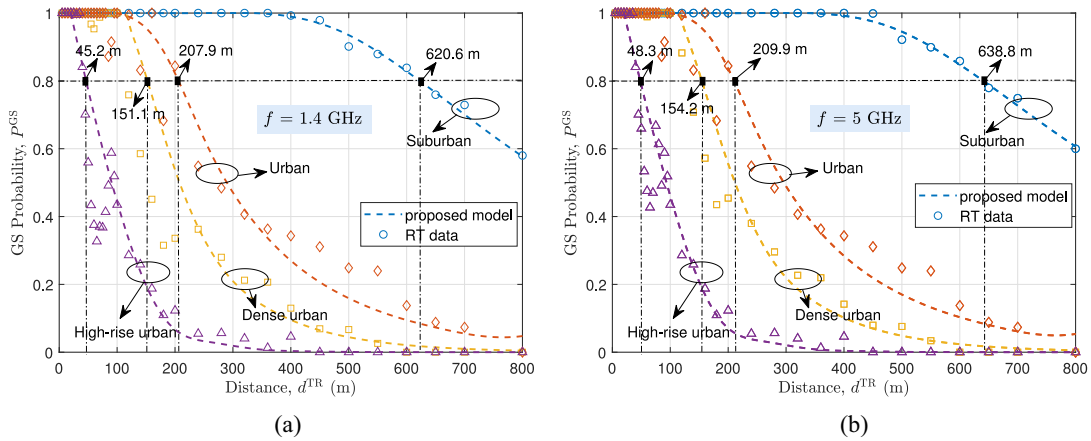


Fig. 7. Comparison of the proposed GS probability model and RT data ( $h^{\text{TR}} = 200$  m). (a) GS probability at  $f = 1.4$  GHz. (b) GS probability at  $f = 5$  GHz.

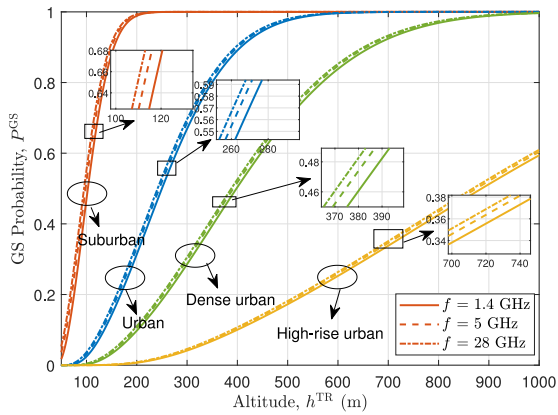


Fig. 8. GS probability versus altitude at different frequencies.

obtained by substituting  $\alpha$  and  $\beta$  into (3) and (4). Moreover, it is assumed that the buildings and streets follow Uniform distribution and the height of buildings obeys Rayleigh distribution. Moreover, 50 TXs with the height from 10 to 1000 m are evenly placed, and 6825 RXs at the altitude of 2 m are uniformly distributed on several concentric circles in each scenario, which covers most of the possible local surrounding conditions. The detailed parameters are given in Table III. It should be mentioned that 28 GHz is one of the recommended bands for 5G millimeter-wave (mmWave) communications [7] and 1.4 GHz is also recommended by China government as the communication frequency of UAV data link.

We apply the RT technique to the constructed scenarios and obtain the conditions of LoS, GS, and BS paths. In this article, the commercial RT tool, Wireless InSite, is adopted in this article to obtain the RT simulation data [44]. The occurrence number of LoS, GS, and BS paths at the same altitude and distance can be obtained, respectively. Then, the path probabilities of LoS, GS, and BS paths refer to the ratio of occurrence number to the total number.

### B. Comparison and Validation

We first analyze and verify the LoS probability model which is described as a function of elevation angle at the

high latitude (over 10 km), as presented in [27] and [35]. In Fig. 2, the elevation angle is defined as  $\theta = \arctan(h^{\text{TR}}/d^{\text{TR}})$  and the proposed LoS probability model can be transformed to the function of  $\theta$ . Set  $f = 28$  GHz,  $h^{\text{TX}} = 5005$  m, and  $h^{\text{RX}} = 5$  m. The comparison results with respect to  $\theta$  for different scenarios are shown in Fig. 6(a). It can be seen that the prediction trend of the proposed model is the same as that of the models in [27] and [35].

The comparison of the proposed LoS probability model, RT simulation method, and the standard models under Urban scenario is shown in Fig. 6(b). Since the standard models are designed for low altitude scenarios, the relative height  $h^{\text{TR}} = h^{\text{TX}} - h^{\text{RX}}$  is set as 30 m. The model in [41] is an altitude-dependent model but assumes the buildings of the Poisson point process (PPP) distribution, so we set the relative height 120 and 500 m. As we can see, the proposed LoS probability model shows good agreement with the standard models and the RT data at low altitude. As the altitude increases, the standard models are no longer applicable. However, our proposed model is still applicable and shows good agreement with the RT data. Note that the LoS path is essential for the reliability of millimeter-wave (mmWave) A2G communications. Taking the LoS probability of 0.9 as an example, we can obtain the average MCDs as 42.8, 139.7, and 503.2 m for different altitudes of UAV. This is because the LoS path is blocked by less buildings as the altitude increases. These quantitative results can be used to evaluate the cell coverage and placement of aerial base stations.

To the best of our knowledge, there are no probability models for the GS and BS paths of A2G channels. To verify the proposed GS probability model, we use the RT results under the aforementioned four urban scenarios. Since the GS and BS paths have more influence on the sub-6G A2G communications, the simulation parameters are set as  $f = 1.4/5$  GHz,  $h^{\text{TX}} = 202$  m, and  $h^{\text{RX}} = 2$  m. As shown in Fig. 7, excellent agreement between the proposed model and RT data verifies the prediction accuracy. Moreover, in the four urban scenarios, the GS path probability gradually decreases with increasing communication distance since longer communication distance involves a larger number of buildings which in turn increases

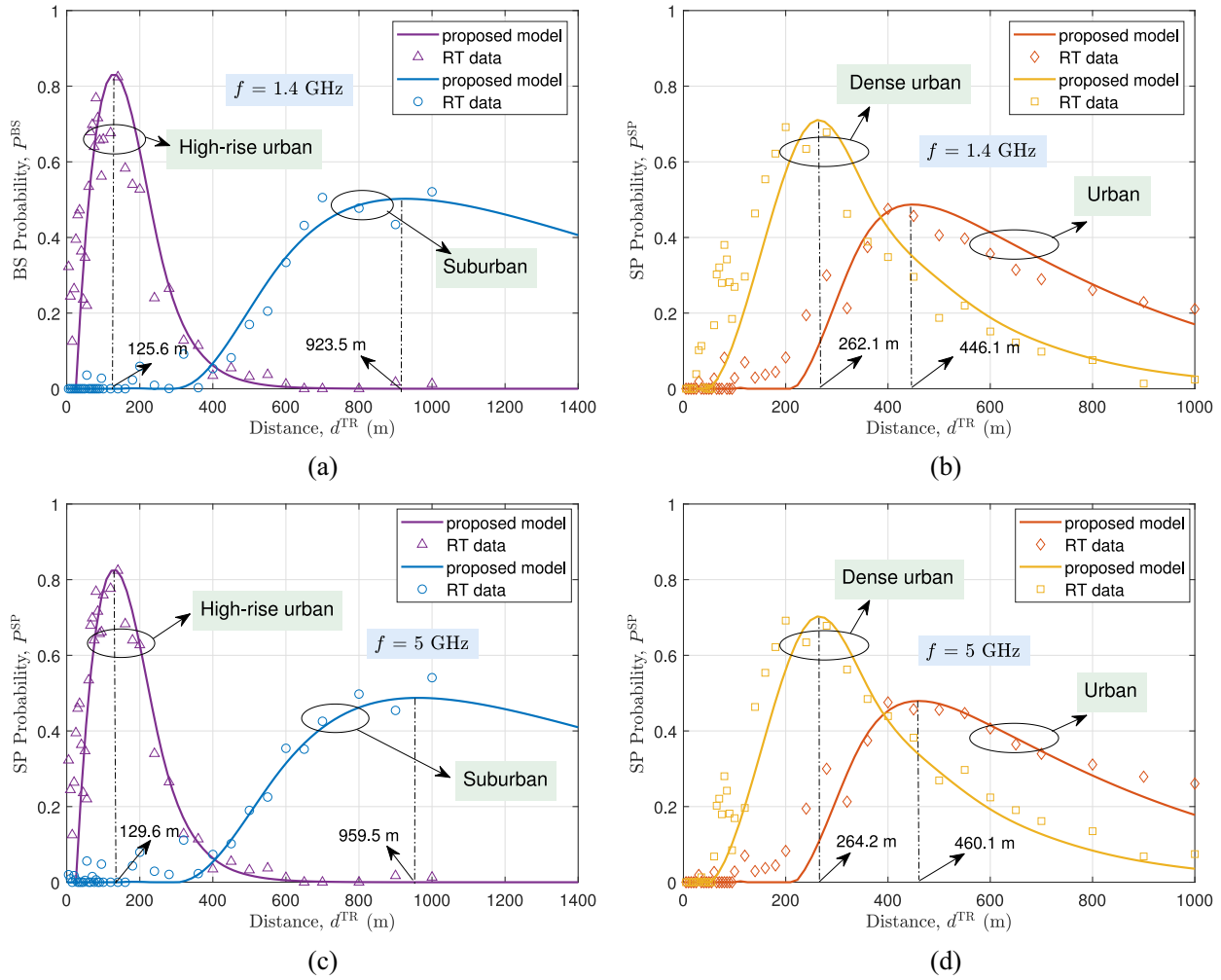


Fig. 9. Comparison of the proposed BS probability model and RT data ( $h^{TR} = 200$  m). (a) Suburban and high-rise urban,  $f = 1.4$  GHz. (b) Urban and dense urban,  $f = 1.4$  GHz. (c) Suburban and high-rise urban,  $f = 5$  GHz. (d) Urban and dense urban,  $f = 5$  GHz.

the probability of occlusion. Taking the GS probability of 0.8 as an example, we can obtain the average MCDs on 1.4 GHz as 651.1, 209.9, 156.2, and 52.5 m for different scenarios. For the case of 5 GHz, the corresponding MCDs are slightly larger. This is because the Fresnel zone radius of 5 GHz is smaller than the one of 1.4 GHz, which makes the valid communication distance a little longer. Furthermore, we give the relationships between the GS probability and UAV altitude with different frequencies under different scenarios in Fig. 8. The GS probability rises as the altitude increases. The reason is that the increase in communication height makes less occlusion of the building height.

To verify the proposed BS probability model, we set  $f = 1.4/5$  GHz,  $h^{TX} = 202$  m, and  $h^{RX} = 2$  m and compare the proposed model with the RT data under four urban scenarios in Fig. 9. We can see that the BS probability increases first and then decreases with the increasing distance. It is shown in (30) that the trend of BS probability is mainly influenced by three factors  $P_i^S$ ,  $P_{i,m}^F$ , and  $P_{i,n}^B$ . For the rising stage,  $P_i^S$ , depending on the scattering building, plays a major role in the BS probability. As the distance increases, the radius of the Fresnel ellipsoid increases. Therefore, the scattering building

is easy to enter the first Fresnel zone, and it makes the value of  $P_i^S$  rise. For the decreasing stage, the point whether the scattering propagation is obstructed by the front and behind buildings refers to  $P_{i,m}^F$  and  $P_{i,n}^B$ . The long distance makes the probability  $P_{i,m}^F$  and  $P_{i,n}^B$  increase significantly. Moreover, as the scenario transforms from Suburban to High-rise urban, the optimal communication distances are 975.8, 470.9, 262.5, and 129.6 m, respectively. This is because the BS path is easy to be blocked when the density of buildings increases. In addition, as the frequency increases, the Fresnel zone radius decreases and the MCD increases.

The prediction results at 1.4 GHz are given in Fig. 10, which demonstrates the effects of altitude on the BS probability. As we can see, scenarios with dense and high buildings, such as the Dense urban and High-rise urban, the BS probability is large when the altitude is high. However, it is difficult to carry out long-distance communication. On the contrary, Suburban and Urban support long-distance communication but are not suitable for the communication with extremely high communication altitudes. Moreover, taking the communication altitude of 200 m as an example, we can easily get the MCDs under four scenarios from Fig. 10 as 930,

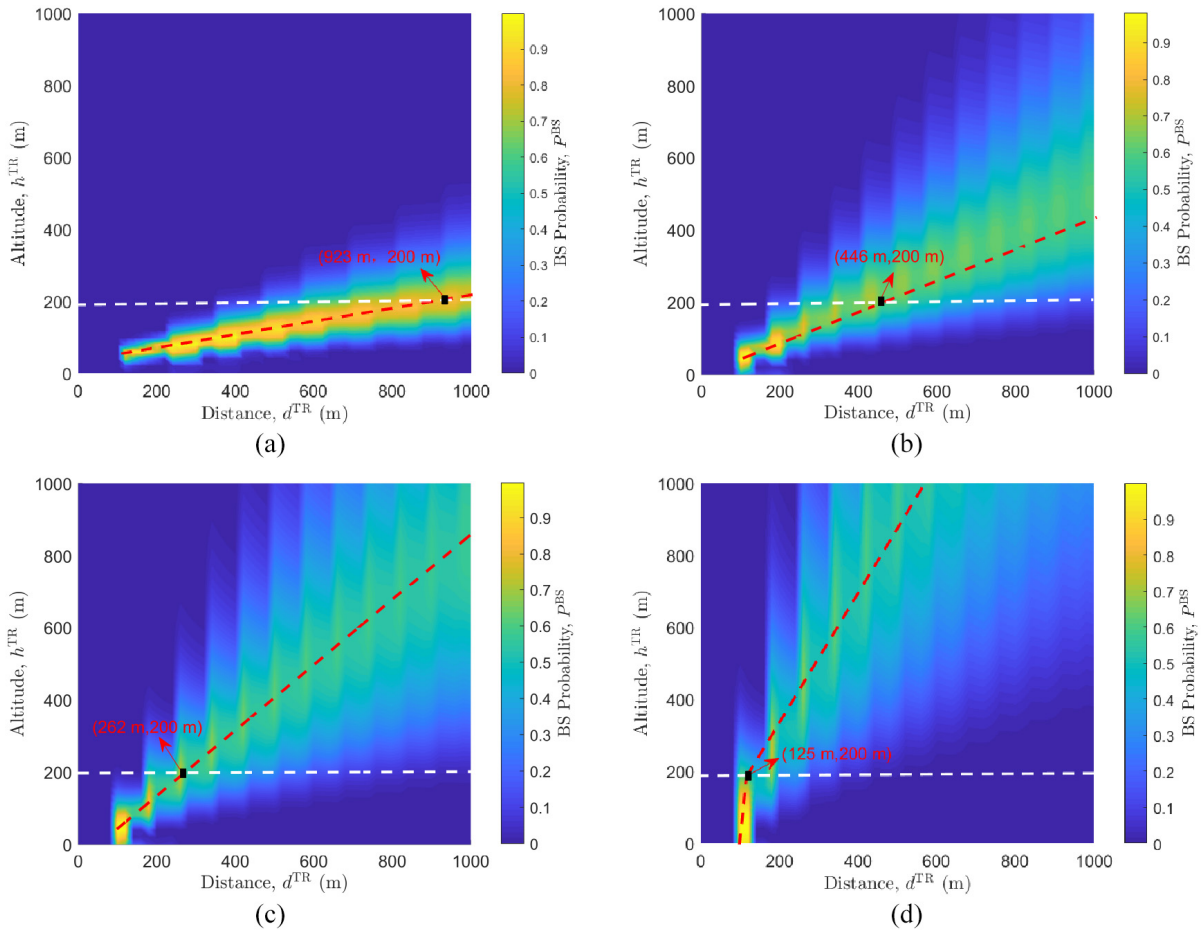


Fig. 10. BS path probabilities with different distances and altitudes ( $f = 1.4$  GHz,  $h^{\text{TR}} = 200$  m). (a) Suburban. (b) Urban. (c) Dense urban. (d) High-rise urban.

446, 262, and 125 m, respectively, which can also be found in Fig. 9.

## V. CONCLUSION

In this article, we have proposed novel stochastic probability models that can predict the occurrence of LoS, GS, and BS paths in A2G communications. These models are based on the stochastic geometric information, i.e., the building height, the building width, and the building locations. The influence of transceiver altitudes, communication distance, and Fresnel ellipsoid zone has also been considered. These models have good versatility in different altitudes and frequencies. Simulation results have shown that the prediction results of LoS, GS, and BS path probabilities are consistent with the RT simulation data and also compatible with the existing probability models for the specific purpose. The research content can be used in enhancing the communication performance, signal coverage, and layout optimization of aerial base stations in the A2G integrated networks.

## REFERENCES

- [1] Z. Xiao, H. Dong, L. Bai, D. O. Wu, and X.-G. Xia, "Unmanned aerial vehicle base station (UAV-BS) deployment with millimeter-wave beamforming," *IEEE Internet Things J.*, vol. 7, no. 2, pp. 1336–1349, Feb. 2020.
- [2] Z. Ma, B. Ai, R. He, G. Wang, Y. Niu, and Z. Zhong, "A wideband non-stationary air-to-air channel model for UAV communications," *IEEE Trans. Veh. Technol.*, vol. 69, no. 2, pp. 1214–1226, Feb. 2020.
- [3] X. Cheng, Y. Li, C.-X. Wang, X. Yin, and D. W. Matolak, "A 3-D geometry-based stochastic model for unmanned aerial vehicle MIMO Ricean fading channels," *IEEE Internet Things J.*, vol. 7, no. 9, pp. 8674–8687, Sep. 2020.
- [4] Y. Liu, H.-N. Dai, Q. Wang, M. K. Shukla, and M. Imran, "Unmanned aerial vehicle for Internet of everything: Opportunities and challenges," *Comput. Commun.*, vol. 155, no. 4, pp. 66–83, Dec. 2020.
- [5] T. Alladi, Naren, G. Bansal, V. Chamola, and M. Guizani, "SecAuthUAV: A novel authentication scheme for UAV-ground station and UAV-UAV communication," *IEEE Trans. Veh. Technol.*, vol. 69, no. 12, pp. 15068–15077, Dec. 2020.
- [6] H. Chang et al., "A novel nonstationary 6G UAV-to-ground wireless channel model with 3-D arbitrary trajectory changes," *IEEE Internet Things J.*, vol. 8, no. 12, pp. 9865–9877, Jun. 2021.
- [7] C.-X. Wang, J. Huang, H. Wang, X. Gao, X. You, and Y. Hao, "6G wireless channel measurements and models: Trends and challenges," *IEEE Veh. Technol. Mag.*, vol. 15, no. 4, pp. 22–32, Dec. 2020.
- [8] B. Li, Z. Fei, and Y. Zhang, "UAV communications for 5G and beyond: Recent advances and future trends," *IEEE Internet Things J.*, vol. 6, no. 2, pp. 2241–2263, Apr. 2019.
- [9] M. Banagar, H. S. Dhillon, and A. F. Molisch, "Impact of UAV wobbling on the air-to-ground wireless channel," *IEEE Trans. Veh. Technol.*, vol. 69, no. 11, pp. 14025–14030, Nov. 2020.
- [10] P. Zhang, J. Li, H. Wang, and X. You, "Millimeter-wave space-time propagation characteristics in urban macrocell scenarios," in *Proc. ICC*, Shanghai, China, 2019, pp. 1–6.
- [11] Q. Zhu et al., "Map-based channel modeling and generation for U2V mmWave communication," *IEEE Trans. Veh. Technol.*, vol. 71, no. 8, pp. 8004–8015, Aug. 2022.

- [12] F. Rinaldi et al., "Broadcasting services over 5G NR enabled multi-beam non-terrestrial networks," *IEEE Trans. Broadcast.*, vol. 67, no. 1, pp. 33–45, Mar. 2021.
- [13] W. Khawaja, I. Guvenc, D. W. Matolak, U.-C. Fiebig, and N. Schneckenburger, "A survey of air-to-ground propagation channel modeling for unmanned aerial vehicles," *IEEE Commun. Surveys Tuts.*, vol. 21, no. 3, pp. 2361–2391, 3rd Quart., 2019.
- [14] X. Cai et al., "An empirical air-to-ground channel model based on passive measurements in LTE," *IEEE Trans. Veh. Technol.*, vol. 68, no. 2, pp. 1140–1154, Feb. 2019.
- [15] S. Ju, Y. Xing, O. Kanhere, and T. S. Rappaport, "Millimeter wave and sub-terahertz spatial statistical channel model for an indoor office building," *IEEE J. Sel. Areas Commun.*, vol. 39, no. 6, pp. 1561–1575, Jun. 2021.
- [16] Q. Zhu et al., "A novel 3D non-stationary wireless MIMO channel simulator and hardware emulator," *IEEE Trans. Commun.*, vol. 66, no. 9, pp. 3865–3878, Sep. 2018.
- [17] Y. Liu, C.-X. Wang, H. Chang, Y. He, and J. Bian, "A novel non-stationary 6G UAV channel model for maritime communications," *IEEE J. Sel. Areas Commun.*, vol. 39, no. 10, pp. 2992–3005, Oct. 2021.
- [18] X. Liang, X. Zhao, S. Li, Q. Wang, and W. Lu, "A 3D geometry-based scattering model for vehicle-to-vehicle wideband MIMO relay-based cooperative channels," *China Commun.*, vol. 13, no. 10, pp. 1–10, Oct. 2016.
- [19] K. Mao et al., "Machine-learning-based 3-D channel modeling for U2V mmWave communications," *IEEE Internet Things J.*, vol. 9, no. 18, pp. 17592–17607, Sep. 2022, doi: [10.1109/JIOT.2022.3155773](https://doi.org/10.1109/JIOT.2022.3155773).
- [20] J. Rodríguez-Piñero, Z. Huang, X. Cai, T. Domínguez-Bolaño, and X. Yin, "Geometry-based MPC tracking and modeling algorithm for time-varying UAV channels," *IEEE Trans. Wireless Commun.*, vol. 20, no. 4, pp. 2700–2715, Apr. 2021.
- [21] W. Li, J. Zhang, X. Ma, Y. Zhang, H. Huang, and Y. Cheng, "The way to apply machine learning to IoT driven wireless network from channel perspective," *China Commun.*, vol. 16, no. 1, pp. 148–164, 2021.
- [22] "Guidelines for evaluation of radio interface technologies for IMT-advanced," ITU-R, Geneva, Switzerland, Rep. ITU-R M.2135-1, Dec. 2009.
- [23] "Study on channel model for frequencies from 0.5 to 100 GHz," 3GPP, Sophia Antipolis, France, 3GPP Rep. TR 38.901 V15.0.0, Jun. 2018.
- [24] "5G channel model for bands up to 100 GHz," 5GCM, Stockholm, Sweden, Rep., Oct. 2016. [Online]. Available: [http://www.5gworkshops.com/5GCM SIG\\_White%20Paper\\_r2dot3.pdf](http://www.5gworkshops.com/5GCM SIG_White%20Paper_r2dot3.pdf)
- [25] *DL1.2 V1.0 WINNER II Channel Models*, Standard IST-4-027756 WINNER II, Nov. 2017.
- [26] W. Li, L. Tian, J. Zhang, and Y. Cheng, "Analysis of base station deployment impact on LOS probability model for 5G indoor scenario," in *Proc. ICC*, Qingdao, China, 2017, pp. 2898–2904.
- [27] J. Holis and P. Pechac, "Elevation dependent shadowing model for mobile communications via high altitude platforms in built-up areas," *IEEE Trans. Antennas Propag.*, vol. 56, no. 4, pp. 1078–1084, Apr. 2008.
- [28] M. K. Samimi, T. S. Rappaport, and G. R. MacCartney, "Probabilistic omnidirectional path loss models for millimeter-wave outdoor communications," *IEEE Wireless Commun. Lett.*, vol. 4, no. 4, pp. 357–360, Aug. 2015.
- [29] J.-H. Lee, J.-S. Choi, and S.-C. Kim, "Cell coverage analysis of 28 GHz millimeter wave in urban microcell environment using 3-D ray tracing," *IEEE Trans. Antennas Propag.*, vol. 66, no. 3, pp. 1479–1487, Mar. 2018.
- [30] M. Pang et al., "Machine learning based altitude-dependent empirical LoS probability model for air-to-ground communications," *Front. Inf. Technol. Electron. Eng.*, vol. 23, pp. 1378–1389, Sep. 2022, doi: [10.1631/FITEE.2200041](https://doi.org/10.1631/FITEE.2200041).
- [31] C. You and R. Zhang, "Hybrid offline-online design for UAV-enabled data harvesting in probabilistic LoS channels," *IEEE Trans. Wireless Commun.*, vol. 19, no. 6, pp. 3753–3768, Jun. 2020.
- [32] D. Townsend, S. D. Walker, A. Sharples, and A. Sutton, "Urban line-of-sight probability for mmWave mobile access and fronthaul transmission hubs," in *Proc. EuCAP*, Dusseldorf, Germany, 2021, pp. 1–5.
- [33] J. Järveläinen, S. L. H. Nguyen, K. Haneda, R. Naderpour, and U. T. Virk, "Evaluation of millimeter-wave line-of-sight probability with point cloud data," *IEEE Wireless Commun. Lett.*, vol. 5, no. 3, pp. 228–231, Jun. 2016.
- [34] *Propagation Data and Prediction Methods for the Design of Terrestrial Broadband Millimetric Aadio Access Systems*, Radiowave Propagation, ITU-R, Geneva, Switzerland, Rec. ITU-R P.1410-2, 2003.
- [35] A. Al-Hourani, S. Kandeepan, and S. Lardner, "Optimal LAP altitude for maximum coverage," *IEEE Wireless Commun. Lett.*, vol. 3, no. 6, pp. 569–572, Dec. 2014.
- [36] I. Mohammed, I. B. Collings, and S. V. Hanly, "Line of sight probability prediction for UAV communication," in *Proc. ICC Workshops*, Montreal, QC, Canada, 2021, pp. 1–6.
- [37] X. Liu, J. Xu, and H. Tang, "Analysis of frequency-dependent line-of-sight probability in 3-D environment," *IEEE Commun. Lett.*, vol. 22, no. 8, pp. 1732–1735, Aug. 2018.
- [38] Z. Cui, K. Guan, C. Briso-Rodríguez, B. Ai, and Z. Zhong, "Frequency-dependent line-of-sight probability modeling in built-up environments," *IEEE Internet Things J.*, vol. 7, no. 1, pp. 699–709, Jan. 2020.
- [39] M. Gapeyenko, D. Moltchanov, S. Andreev, and R. W. Heath, "Line-of-sight probability for mmWave-based UAV communications in 3D urban grid deployments," *IEEE Trans. Wireless Commun.*, vol. 20, no. 10, pp. 6566–6579, Oct. 2021.
- [40] Q. Zhu et al., "Geometry-based stochastic line-of-sight probability model for A2G channels under urban scenarios," *IEEE Trans. Antennas Propag.*, vol. 70, no. 7, pp. 5784–5794, Jul. 2022.
- [41] A. Al-Hourani, "On the probability of line-of-sight in urban environments," *IEEE Wireless Commun. Lett.*, vol. 9, no. 8, pp. 1178–1181, Aug. 2020.
- [42] S. Roy and M. Mehrnosh, "A new Poisson process-based model for LOS/NLOS discrimination in clutter modeling," *IEEE Trans. Antennas Propag.*, vol. 67, no. 12, pp. 7538–7549, Dec. 2019.
- [43] A. Al-Hourani, S. Kandeepan, and A. Jamalipour, "Modeling air-to-ground path loss for low altitude platforms in urban environments," in *Proc. GLOBECOM*, Austin, TX, USA, 2014, pp. 2898–2904.
- [44] "Wireless insite 3D wireless prediction software." Remcom. Accessed: May 20, 2020. [Online]. Available: <https://www.remcom.com/wireless-insite-em-propagation-software>



**Minghui Pang** received the B.S. degree in information engineering from Nanjing University of Aeronautics and Astronautics, Nanjing, China, in 2020, where she is currently pursuing the M.S. degree in electronic science and technology.

Her research interests include channel modeling and unmanned aerial vehicles communication systems.



**Qiuming Zhu** (Member, IEEE) received the B.S. degree in electronic engineering and the M.S. and Ph.D. degrees in communication and information system from Nanjing University of Aeronautics and Astronautics (NUAA), Nanjing, China, in 2002, 2005, and 2012, respectively.

Since 2021, he has been a Professor with the Department of Electronic Information Engineering, NUAA. From October 2016 to October 2017, from June 2018 to August 2018, and from June 2018 to August 2018, he was also an Academic Visitor with Heriot-Watt University, Edinburgh, U.K. He has authored or coauthored more than 120 articles in refereed journals and conference proceedings and holds over 40 patents. His current research interests include channel sounding, modeling, and emulation for the fifth/sixth generation mobile communication, vehicle-to-vehicle communication, and unmanned aerial vehicles communication systems.



**Cheng-Xiang Wang** received the B.Sc. and M.Eng. degrees in communication and information systems from Shandong University, Jinan, China, in 1997 and 2000, respectively, and the Ph.D. degree in wireless communications from Aalborg University, Aalborg, Denmark, in 2004.

He was a Research Assistant with Hamburg University of Technology, Hamburg, Germany, from 2000 to 2001, a Research Fellow with the University of Agder, Grimstad, Norway, from 2001 to 2005, and a Visiting Researcher with Siemens AG Mobile Phones, Munich, Germany, in 2004. He has been with Heriot-Watt University, Edinburgh, U.K., since 2005, where he was promoted to a Professor in 2011. In 2018, he joined the National Mobile Communications Research Laboratory, Southeast University, Nanjing, China, as a Professor. He is currently a part-time Professor with Purple Mountain Laboratories, Nanjing. He has authored four books, three book chapters, and more than 420 articles in refereed journals and conference proceedings, including 24 highly cited articles. He has delivered 22 invited keynote speeches/talks and eight tutorials in international conferences. His current research interests include wireless channel measurements and modeling, 6G wireless communication networks, and applying artificial intelligence to wireless networks.

Prof. Wang received 12 Best Paper Awards from IEEE GLOBECOM 2010, IEEE ICCT 2011, ITST 2012, IEEE VTC 2013-Spring, IWCMC 2015, IWCMC 2016, IEEE/CIC ICC 2016, WPMC 2016, WOCC 2019, IWCMC 2020, and WCSP 2020. He has served as a TPC member, the TPC chair, and the general chair for more than 80 international conferences. He has served as an Editor for nine international journals, including the IEEE TRANSACTIONS ON WIRELESS COMMUNICATIONS from 2007 to 2009, the IEEE TRANSACTIONS ON VEHICULAR TECHNOLOGY from 2011 to 2017, and the IEEE TRANSACTIONS ON COMMUNICATIONS from 2015 to 2017. He was a Guest Editor of the IEEE JOURNAL ON SELECTED AREAS IN COMMUNICATIONS, Special Issue on Vehicular Communications and Networks (a Lead Guest Editor), Special Issue on Spectrum and Energy Efficient Design of Wireless Communication Networks, and Special Issue on Airborne Communication Networks. He was also a Guest Editor of the IEEE TRANSACTIONS ON BIG DATA, Special Issue on Wireless Big Data, and is a Guest Editor for the IEEE TRANSACTIONS ON COGNITIVE COMMUNICATIONS AND NETWORKING, Special Issue on Intelligent Resource Management for 5G and Beyond. He is an Executive Editorial Committee Member for the IEEE TRANSACTIONS ON WIRELESS COMMUNICATIONS. He was an IEEE Communications Society Distinguished Lecturer in 2019 and 2020. He is a member of the Academia Europaea, a Fellow of IET, and a Highly Cited Researcher recognized by Clarivate Analytics in 2017–2020.



**Zhipeng Lin** (Member, IEEE) received the Ph.D. degrees from the School of Information and Communication Engineering, Beijing University of Posts and Telecommunications, Beijing, China, and the School of Electrical and Data Engineering, University of Technology Sydney, Ultimo, NSW, Australia, in 2021.

He is currently an Associate Researcher with the College of Electronic and Information Engineering, Nanjing University of Aeronautics and Astronautics, Nanjing, China. His current research interests include signal processing, massive MIMO, spectrum sensing, and UAV communications.



**Junyu Liu** (Member, IEEE) received the B.Eng. and Ph.D. degrees in communication and information systems from Xidian University, Xi'an, China, in 2007 and 2016, respectively.

He is currently a Lecturer and a Postdoctoral Researcher with the State Key Laboratory of Integrated Service Networks, Institute of Information and Science, Xidian University. His research interests include interference management and performance evaluation of wireless heterogeneous networks and ultradense wireless networks.



**Chongyu Lv** received the B.S. degree in communication engineering from Nanjing University of Posts and Telecommunications, Nanjing, China, in 2022, where he is currently pursuing the M.S. degree in communication and information systems.

His research interests include channel modeling and modeling for UAV.



**Zhuo Li** (Member, IEEE) received the B.Sc. degree in electronic engineering and the M.E. degree in electromagnetic fields and microwave techniques from Nanjing University of Aeronautics and Astronautics (NUAA), Nanjing, China, in 2001 and 2004, respectively, and the Ph.D. degree in radio engineering from the State Key Laboratory of Millimeter Waves, Southeast University, Nanjing, in 2009.

From 2015 to 2016, he was a Visiting Scholar with the Department of Physics, Arizona State University, Tempe, AZ, USA. He is currently a Full Professor with the College of Electronic and Information Engineering, NUAA. He has authored or coauthored over 120 papers in refereed journals and conference proceedings, including *Advanced Science*, *Advanced Optical Materials*, *Nano Letters*, *Physical Review Applied*, IEEE TRANSACTIONS ON MICROWAVE THEORY AND TECHNIQUES, IEEE TRANSACTIONS ON ANTENNAS AND PROPAGATION, and IEEE TRANSACTIONS ON ELECTROMAGNETIC COMPATIBILITY. He has filed more than 30 patents. His current research interests include plasmonic metamaterials, MHz-through-THz technologies and transceivers for wireless sensors and biomedical applications, and electromagnetic compatibility in avionics system and auto electrical system. He is also interested in the modeling and design of microwave and terahertz photonic circuits and systems.

Prof. Li received the Second Prize of Natural Science of China Institute of Electronics in 2019 and the NUAA Outstanding Undergraduate Teaching Promotion Award in 2019. He is on the Advisory Board for *Journal of Physics D: Applied Physics* and on the Review Board for many international journals, including *ACS Photonics*, *Nanotechnology*, *Nano-Micro Letters*, IEEE TRANSACTIONS ON MICROWAVE THEORY AND TECHNIQUES, IEEE TRANSACTIONS ON ANTENNAS AND PROPAGATION, and IEEE TRANSACTIONS ON ELECTROMAGNETIC COMPATIBILITY. He also served as the invited speaker and the session chair in many international conferences and workshops. He is a Senior Member of the Chinese Institute of Electronics and a Committee Member of the Antenna Branch of Chinese Institute of Electronics.